

# Self-Supervision & Meta-Learning for One-Shot Unsupervised Cross-Domain Detection

Francesco Cappio Borlino<sup>a,b,✉</sup>, Salvatore Polizzotto<sup>a</sup>, Antonio D’Innocente<sup>c</sup>, Silvia Bucci<sup>a</sup>, Barbara Caputo<sup>a</sup>, Tatiana Tommasi<sup>a,b</sup>

<sup>a</sup>Politecnico di Torino, Corso Duca degli Abruzzi 24, 10129 Torino, Italy

<sup>b</sup>Italian Institute of Technology, Italy

<sup>c</sup>Sapienza University of Rome, Italy

## ABSTRACT

Deep detection approaches are powerful in controlled conditions, but appear brittle and fail when source models are used off-the-shelf on unseen domains. Most of the existing works on domain adaptation simplify the setting and access jointly both a large source dataset and a sizable amount of target samples. However this scenario is unrealistic in many practical cases as when monitoring image feeds from social media: only a pretrained source model is available and every target image uploaded by the users belongs to a different domain not foreseen during training. We address this challenging setting by presenting an object detection algorithm able to exploit a pre-trained source model and perform unsupervised adaptation by using only one target sample seen at test time. Our multi-task architecture includes a self-supervised branch that we exploit to meta-train the whole model with single-sample cross-domain episodes, and prepare to the test condition. At deployment time the self-supervised task is iteratively solved on any incoming sample to one-shot adapt on it. We introduce a new dataset of social media image feeds and present a thorough benchmark with the most recent cross-domain detection methods showing the advantages of our approach.

## 1. Introduction

Despite impressive progress in object detection over the last years, reliably localizing and recognizing objects across visual domains is still an open problem. Indeed, most of the existing detectors rely on deep features learned from large amount of labeled training data usually drawn from a specific *source* distribution and suffer from severe performance degradation when applied on images sampled from a different *target* domain. This hinders the deployment of detection models in real-world conditions. Consider for example the task of social media monitoring (see Figure 1): the images are posted on multiple platforms by a large variety of users, each with his/her own personal taste in the choice of style and post-processing filters which may change in time. Even when images contain instances of the same object category, they are acquired in different contexts, under different viewpoints and illumination conditions. In other words, *each image comes from a different visual domain, distinct from the visual domain where the detector has been*

*trained*. This scenario poses several key challenges: (1) the annotated source images on which a detector is learned might be proprietary and not accessible at deployment time; (2) the prediction should be provided on every new sample: waiting to collect a sizable amount of target data, identifying the shared domain, and then adapting to it is not feasible; (3) even when the application allows to use this target batching strategy, it is not recommended because there is no guarantee that the images received from time  $t+1$  will come from the same target domain of those observed up to time  $t$ . Our work addresses this setting that we named *One-Shot Unsupervised Cross-Domain Detection* in (D’Innocente et al., 2020). The method OSHOT proposed in the same work exploited self-supervised learning as an auxiliary task while training the detection model. Given a new target sample, pseudo-labeling was used to locate region of interest on which the self-supervised objective could be finetuned, updating the internal feature representation before the final prediction. Here we extend our previous work in several directions. (1) We present a novel meta-learning formulation to combine the main supervised detection task with the self-supervised auxiliary objective. It prepares the source model to be effectively transferred on one single sample, finally producing good results

✉Corresponding author:

e-mail: francesco.cappio@polito.it (Francesco Cappio Borlino)

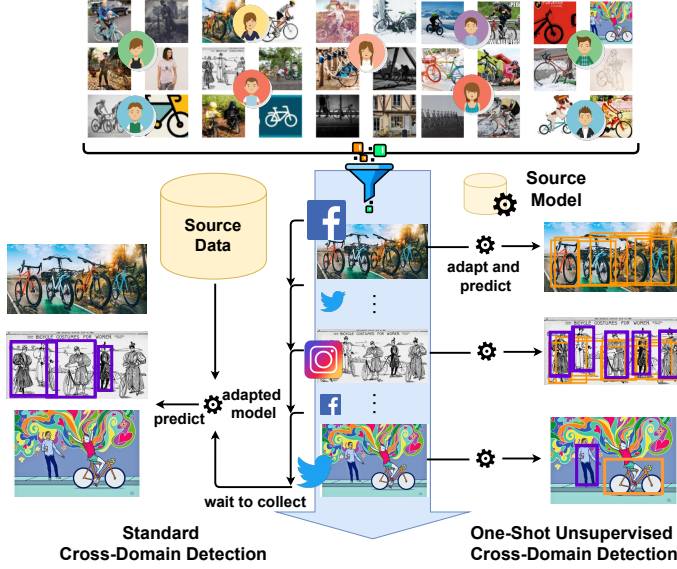


Fig. 1: Social media images comes from different users and domains: at the top we show a subset of the Social Bikes dataset that we collected from Facebook, Instagram and Twitter. Existing cross-domain detection algorithms (left) struggle to adapt in this scenario because they need to collect a batch of target samples and access source data. In one-shot unsupervised cross-domain detection (right), we start from a pretrained source model which is adapted on a single target image and predicts on it.

after a few adaptation iterations on it. We indicate it as FULL-OSSHOT. As well as OSSHOT, the new variant does not need access to the source data at test time. (2) We define a tailored experimental setup by introducing a new test dataset collected from social media feeds. (3) We run an extensive benchmark evaluation comparing with the most recent adaptive detection algorithms (Saito et al., 2019; Kim et al., 2019b; Xu et al., 2020; Wu et al., 2021) and one-shot style-transfer based unsupervised learning approach (Cohen and Wolf, 2019), achieving the new state-of-the-art. (4) Our study includes a detailed error analysis via the toolbox proposed in (Bolya et al., 2020) and thorough ablation experiments to assess the role of all the inner components of our approach.

## 2. Related Work

**Cross-Domain Object Detection.** Existing deep learning based object detectors perform remarkably well (Ren et al., 2015; Lin et al., 2017), however their robustness across visual domains remains a major issue. Unsupervised domain adaptation methods attempt to close the domain gap between the annotated source on which learning is performed, and the target samples on which the model is deployed. The standard adaptive setting assumes the availability of all the unlabeled target test data at training time. One adaptive strategy consists in including *feature alignment* modules at different internal stages of the deep architecture (Chen et al., 2018). The Strong-Weak method (SW, Saito et al. (2019)) proposed a balanced alignment with strong global and weak local feature adaptation. The SW-ICR-CCR method (Xu et al., 2020) includes an image-level multi-label classifier and a module imposing consistency between the image-level and instance-level predictions. The re-

cent approach ICCR-VDD (Wu et al., 2021) exploits vector decomposition to separate domain-invariant and domain-specific representation with the former used to extract object proposals. Another group of works developed *pixel-level adaptation* methods which modify source images to resemble those of the target. The Domain-Transfer approach (DT, Inoue et al. (2018)) was the first to apply this strategy for object detection. More recently Div-Match (Kim et al., 2019b) re-elaborated the idea of domain randomization (Tobin et al., 2017) to produce three extra source variants with which the target can be aligned through an adversarial multi-domain discriminator. Finally, pseudo-labeling, also known as *self-training*, is often used as an adaptation technique: the output of the source detector serves as a coarse annotation for the unlabeled target samples which are included in the supervised training (Kim et al., 2019a; Khodabandeh et al., 2019).

**Adaptive Learning on a Budget.** When dealing with domain shift, learning on a target budget becomes extremely challenging. Only few attempts have been done to reduce the target cardinality. Motiian et al. (2017) considered *few-shot supervised domain adaptation* where the few target samples available are fully labeled. Cohen and Wolf (2019) focused on *one-shot unsupervised style transfer* with a large source dataset and a single unsupervised target image. They developed a time-costly autoencoder-based method whose goal is image generation with no discriminative purpose. A related scenario is that of *online domain adaptation* where unsupervised target samples belong to a single coherent domain and are initially scarce, but accumulate in time (Hoffman et al., 2014; Mancini et al., 2018).

**Self-Supervised Learning.** Unlabeled data is rich in structural information and self-supervised learning aims at capturing it, to then serve as a pre-training step for different downstream tasks. Recently Asano et al. (2020) have shown the potential of a model learned by self-supervision from a single image. Several works have also indicated that self-supervision supports generalization when combined with supervised learning in a multi-task framework (Bucci et al., 2021; Xu et al., 2019; Alliego et al., 2021).

**Meta-Learning.** The objective of meta-learning is to enable a model for fast adaptability. A well known strategy is that proposed by Finn et al. (2017): the *inner* learning loop solves a standard supervised task, while the *outer* meta-learning loop updates the base model by observing multiple episodes of the standard task to accomplish a higher level objective as generalization or increasing learning speed. This technique allows adaptation to novel tasks with scarce supporting examples and has been largely used for few-shot learning (Snell et al., 2017; Vinyals et al., 2016; Rusu et al., 2019). Various kind of meta-knowledge as losses (Li et al., 2019), regularization functions (Balaji et al., 2018) and data augmentation (Tseng et al., 2020) can be (meta) learned to maximize the model robustness by using a validation domain different from the training one.

**Our approach for one shot unsupervised cross-domain detection relates to learning on a budget and connects to the few-shot meta-learning literature.** Specifically we leverage meta-learning by simulating multiple unsupervised single-sample cross-domain learning episodes for the multi-

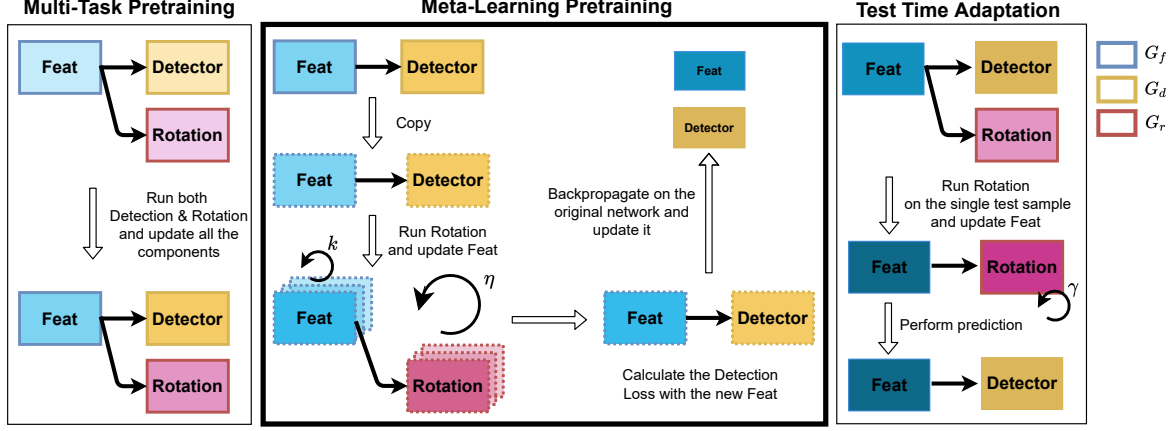


Fig. 2: Visualization of the complete FULL-OSHOT proposed approach. The first phase, inherited from OSHOT, is a multi-task pretraining in which all the modules are updated through the rotation and detection losses. The second pretraining stage, introduced for FULL-OSHOT, exploits a meta-learning with the rotation recognition as the inner optimization task to prepare the network for the test-time adaptation stage. In this last phase both the rotation and feature extractor modules are updated by performing the self-supervised task iteratively on a single test sample. The adapted feature extractor is finally used to predict on the same test image. Each change in color shades indicates an update of a module. We use dotted lines to highlight the components optimized in the meta-learning loop.

task model that integrates a self-supervised and a supervised objective. The designed method is source-free, meaning that the test-time adaptation does not need access to the source data.

### 3. Method

Starting from  $N$  annotated samples of the source domain  $S = \{x_i, y_i\}_{i=1}^N$ , we want to perform detection on a single image  $x^t$ , with  $t$  being any target domain not available at training time. Here the structured labels  $y = (c, b)$  describe class identity  $c$  and bounding box location  $b$  in each image  $x$ . To pursue the described goal, our strategy is to train the parameters of a detection learning model such that it can be ready to get the maximal performance on a single unsupervised sample from a new domain after few gradient update steps on it.

In (D’Innocente et al., 2020) we designed OSHOT: a deep multi-task method that included a *pretraining* and an *adaptation* phase. The former involves the source, optimizing jointly the detection and an auxiliary self-supervised rotation recognition objective. In the latter stage the network features are updated on the single target sample by focusing only on the rotation task before performing a prediction. Moreover, the approach exploits *self-training* in a *cross-task* fashion so that the auxiliary rotation focuses on the selected object area. The basic detector is Faster R-CNN (Ren et al., 2015), that has three main components: an initial block of convolutional layers, a region proposal network (RPN) and a region-of-interest (ROI) based classifier. The bottom layers transform any input image  $x$  into its convolutional feature map  $G_f(x|\theta_f)$  where  $\theta_f$  parametrizes the feature extraction model. The feature map is then used by RPN to generate candidate object proposals. Finally the ROI-wise classifier  $G_d(\cdot|\theta_d)$  predicts the category label and object position from the feature vector obtained via ROI-pooling.

**Multi-task Pretraining** (Figure 2, left). The detection head and the feature extractor are trained jointly using a loss function  $\mathcal{L}_d(G_d(G_f(x|\theta_f)|\theta_d), y)$  which evaluates cost errors for both object classification and regression of the identified bounding boxes.

For the auxiliary rotation task, each training image  $x$  is transformed via a rotation operator  $R(x, \alpha)$ , where  $\alpha = q \times 90^\circ$  indicates the orientation with  $q \in \{0, \dots, 3\}$ . We indicate the obtained set of samples as  $\{R(x)_j, q_j\}_{j=1}^M$ , where we dropped the  $\alpha$  for simplicity. We indicate the auxiliary rotation classifier and its parameters respectively with  $G_r$  and  $\theta_r$ .

The overall objective of the multi-task designed model is:

$$\arg \min_{\theta_f, \theta_d, \theta_r} \mathcal{L}_d(G_d(G_f(x|\theta_f)|\theta_d), y) + \lambda \mathcal{L}_r(G_r(G_f(R(x)|\theta_f)|\theta_r), q), \quad (1)$$

where  $\mathcal{L}_r$  is the cross-entropy loss. In this way, the shared feature map  $G_f(x|\theta_f)$  is learned under the synchronous guidance of both the detection and rotation objectives. We designed  $G_r$  by exploiting the ground truth location of each object and selecting features from its bounding box in the original map  $G_r(\cdot|\theta_r) = \text{FC}_{\theta_r}(\text{boxcrop}(\cdot))$ . The *boxcrop* operation includes pooling to rescale the feature dimension before entering the final FC layer. In this way the network is encouraged to focus only on the object orientation without introducing noisy information from the background. We randomly pick one rotation angle per instance.

**Meta-Learning Pretraining** (Figure 2, center). Multi-task learning is appealing for deep learning regularization and including a self-supervised task has the advantage of waiving any extra data annotation cost. Still, our main interest remains on detection, while rotation recognition should be considered as a secondary task. To manage this role for rotation, and to better fit to the unlabeled one-shot scenario on a new domain faced at test time, we re-formulate the OSHOT model inspired by meta-learning and building over the bi-level optimization process of MAML (Finn et al., 2017). Specifically we propose to meta-train the detection model with the rotation task as its inner base learner. The optimization objective can be written as

$$\begin{aligned} & \arg \min_{\theta_f, \theta_d} \frac{1}{K} \sum_{k=1}^K \mathcal{L}_d(G_d(G_f(x_k|\theta_f')|\theta_d), y) \\ & \text{s.t. } (\theta_f', \theta_r') = \arg \min_{\theta_f, \theta_r} \mathcal{L}_r(G_r(G_f(R(x_k)|\theta_f')|\theta_r), q). \end{aligned} \quad (2)$$

**Algorithm 1: Meta-Learning on one source sample**


---

**Input:**  $G_f, G_d, G_r$ , parameters  $\theta_f, \theta_d, \theta_r$ , rotator  $R$ , augmenter  $A$   
**Data:** Source image  $x$  with  $y = (b, c)$

- 1 **while** still  $k$  augmentations **do**
- 2    $x_k \leftarrow A(x)$
- 3    $(\theta'_f, \theta'_r) \leftarrow (\theta_f, \theta_r)$  ▷ copy params
- 4   **while** still  $\eta$  iterations **do**
- 5      $\tilde{b}, \tilde{c} \leftarrow G_d(G_f(x_k | \theta'_f) | \theta_d)$
- 6      $x_{r,k} \leftarrow R(x_k)$  ▷ rand. rotation  $q$
- 7      $b_{r,k} \leftarrow R(\tilde{b})$
- 8     minimize self-supervised loss
- 9      $(\theta'_f, \theta'_r) \leftarrow (\theta'_f, \theta'_r) - \alpha \nabla_{\theta'_f, \theta'_r} \mathcal{L}_r(G_r(G_f(b_{r,k} | \theta'_f) | \theta'_r), q)$   
▷  $G_r(\cdot | \theta'_r) = FC_{\theta'_r}(\text{pseudoboxcrop}(\cdot))$
- 10  **end**
- 11  compute the supervised loss  $l_k = \mathcal{L}_d(G_d(G_f(x_k | \theta'_f) | \theta_d), y)$
- 12 **end**
- 13 minimize the supervised loss
- 14  $(\theta^*_f, \theta^*_d) \leftarrow (\theta_f, \theta_d) - \beta \nabla_{\theta_f, \theta_d} \sum_{k \in K} l_k$

---

In words, we start by focusing on the rotation recognition task for each source sample  $x$  after augmenting it in  $k = 1, \dots, K$  different ways. We consider semantic-preserving augmentations (e.g. gray-scale, color jittering) and perform multiple learning iterations ( $\eta$  gradient-based update steps). This optimization, whose learning objective is reported in the second row of Equation (2), leads to the update of the feature extractor and rotation classification modules (parameters  $\theta'_f$  and  $\theta'_r$ ). The outer meta-learning loop, whose learning objective is in first row of Equation (2), leverages on it to optimize the detection model over all the  $K$  data variants and prepares for generalization and fine-tuning on a single sample. To simulate the deployment setting we neglect the ground truth object location for the inner rotation objective and in  $G_r$  we substitute the *boxcrop* with *pseudoboxcrop* obtained through the cross-task self-training procedure detailed in the following paragraph.

**Cross-task self-training.** Instead of following the self-training standard practice which consists in using the pseudo-labels produced by the source model on the target to update the detector, we exploit them for the self-supervised rotation classifier. With this cross-task self-training we keep the advantage of the self-training initialization while largely reducing the risks of error propagation due to wrong class pseudo-labels. We start from the  $(\theta_f, \theta_d)$  model parameters of the pretraining stage and we get the feature maps from all the rotated versions of the sample  $x$ ,  $G_f(\{R(x, q) | \theta_f\}, q = 0, \dots, 3)$ . Only the feature map produced by the original image (i.e.  $q = 0$ ) is provided as input to the RPN and ROI network components to get the predicted detection  $\tilde{y} = (\tilde{c}, \tilde{b}) = G_d(G_f(x | \theta_f) | \theta_d)$ . This pseudo-label is composed by the class label  $\tilde{c}$  and the bounding box location  $\tilde{b}$ . We discard the first and consider only the second to localize the region containing an object in all the four feature maps, also recalibrating the position to compensate for the orientation of each map. The *pseudoboxcrop* operation is used both in the meta-learning phase and in the adaptation one.

**Test Time Adaptation** (Figure 2, right). Given the single target image  $x^t$ , we adapt on it the original backbone’s parameters  $\theta_f$

**Algorithm 2: Adaptive phase on one target sample**


---

**Input:**  $G_f, G_d, G_r$ , parameters  $\theta_f, \theta_d, \theta_r$ , from the pretraining phase, rotator  $R$   
**Data:** Target image  $x^t$

- 1  $(\theta^*_f, \theta^*_r) \leftarrow (\theta_f, \theta_r)$  ▷ copy params
- 2 **while** still  $\gamma$  iterations **do**
- 3    $\tilde{b}^t, \tilde{c}^t \leftarrow G_d(G_f(x^t | \theta^*_f) | \theta_d)$
- 4    $x_r^t \leftarrow R(x^t)$  ▷ rand. rotation  $q$
- 5    $b_r^t \leftarrow R(\tilde{b}^t)$
- 6   minimize self-supervised loss
- 7    $(\theta^*_f, \theta^*_r) \leftarrow (\theta^*_f, \theta^*_r) - \alpha \nabla_{\theta^*_f, \theta^*_r} \mathcal{L}_r(G_r(G_f(b_r^t | \theta^*_f) | \theta^*_r), q)$   
▷  $G_r(\cdot | \theta^*_r) = FC_{\theta^*_r}(\text{pseudoboxcrop}(\cdot))$
- 8 **end**
- 9 final detection prediction using update parameters
- 10  $y^{t*} = G_d(G_f(x^t | \theta^*_f) | \theta_d)$ .

---

by finetuning the rotation recognition through

$$\arg \min_{\theta_f, \theta_r} \mathcal{L}_r(G_r(G_f(R(x^t) | \theta_f) | \theta_r), q^t). \quad (3)$$

This process involves only  $G_f$  and  $G_r$ , while the RPN and ROI detection components described by  $G_d$  remain unchanged. In the following we use  $\gamma$  to indicate the number of gradient steps (i.e. iterations), with  $\gamma = 0$  corresponding to the pretraining phase. At the end of the finetuning process, the inner feature model is described by  $\theta^*_f$  and the detection prediction on  $x^t$  is obtained by  $y^{t*} = G_d(G_f(x^t | \theta^*_f) | \theta_d)$ .

In the following we indicate with FULL-OSHOT<sup>1</sup> our model exploiting meta-learning pretraining. The meta-learning strategy is summarized in Algorithm 1, while the adaptation process on a single target sample is outlined in Algorithm 2. We also consider two intermediate cases: *Tran-OSHOT* extends OSHOT with the data semantic-preserving transformations used in FULL-OSHOT, and *Meta-OSHOT* corresponds to FULL-OSHOT without transformations (i.e.  $K = 1$ ).

## 4. Experiments

**Dataset and Competitors.** We run an extensive experimental analysis on several datasets. The *Pascal Visual Object Classes (VOC)* Pascal-VOC (Everingham et al., 2010) is a real-world image collection covering bounding boxes annotations for 20 common categories. The *Artistic Media Datasets (AMD)* is composed of Clipart1k, Comic2k and Watercolor2k (Inoue et al., 2018). The first shares its 20 categories with VOC. The other two contain a 6 class subset of VOC. *Cityscapes* (Cordts et al., 2016) is an urban street scene dataset with pixel level annotations of 8 categories from which it is possible to obtain the corresponding bounding boxes as in (Chen et al., 2018). *Foggy Cityscapes* (Sakaridis et al., 2018) contains different levels of synthetic fog over Cityscapes. We consider images with the highest amount of artificial fog. Finally, *Social Bikes* is our new dataset containing 530 images of scenes with persons/bicycles

<sup>1</sup>Code, implementation details and qualitative results are available at <https://github.com/FrancescoCappio/OSHOT-meta-learning>.

collected from Twitter, Instagram and Facebook by searching for `#bike` tags. It is designed to be used as target when the source domain is VOC, indeed the two classes person and bicycles are shared among them.

To run all the experiments we resized the image’s shorter side to 600 pixels and apply random horizontal flipping during pre-training. The detection performance (mAP) is assessed with IoU threshold at 0.5. In the following we use *Source* → *Target* to indicate the experimental setting and report the average of three independent runs. Our detailed error analysis is obtained via TIDE (Bolya et al., 2020): it estimates how much each type of detection error contributes to the missing mAP. It counts false positives and false negatives, and classifies all the errors into six categories. *Cl*s means object localized correctly ( $IoU_{max} \geq 0.5$ ) but classified incorrectly, *Loc* means object classified correctly but localized incorrectly ( $0.1 \leq IoU_{max} < 0.5$ ). *Both* is used when the two situations occur simultaneously. In *Dupe* the detection is correct, but the same ground truth bounding box was already associated with another higher scoring detection. *Bkg* means detected background as foreground ( $IoU_{max} < 0.1$ ) and *Miss* is for all the undetected ground truth boxes not covered by other types of errors.

Our *Baseline* is Faster-RCNN trained on the source domain and deployed on the target without further adaptation. *Tran-Baseline* is a variant obtained by applying at training time the same data semantic-preserving transformations introduced in FULL-OSHOT. This allows us to assess how much of the improvement is due to the higher data variability rather than to the training strategy. We chose as benchmark methods *DivMatch* (Kim et al., 2019b), *SW* (Saito et al., 2019), *SW-ICR-CCR* (Xu et al., 2020) and *ICCR-VDD* (Wu et al., 2021) already described in Section 2. In all the cases we use a ResNet-50 backbone pre-trained on ImageNet for fair comparison. We remark that the cross-domain algorithms need target data in advance and are not designed to work in our one-shot unsupervised setting, thus we provide them with the advantage of at least ten target images accessible during training and randomly selected at each run. We collect average precision statistics during inference.

**Adapting to social feeds.** When the data comes from multiple providers, the assumption that all target images originate from the same underlying distribution does not hold and standard cross-domain detection methods are penalized regardless of the number of seen target samples. We pretrain the source detector on VOC, and deploy it on Social Bikes.

In Table 1 the mAP results with  $\gamma = 0$  allow us to compare the pretraining models before adaptation and already shows the advantage of FULL-OSHOT over OSHOT, as well as over the *Tran* and *Meta* variants. When  $\gamma = 5$  all variants of OSHOT obtain an improvement that ranges from 1.9 (OSHOT) to 2.6 (FULL-OSHOT) points over the Baseline just by adapting on a single test sample. Despite granting them access to the whole set of adaptation samples, the reference domain adaptive algorithms reach at best an advantage of 1.2 points over FULL-OSHOT. When using only ten target samples, half of the methods show a negative transfer w.r.t. the Baseline.

By looking at the detection error analysis we can see that the adaptation iterations allow OSHOT to reduce the number

Table 1: Results for VOC → Social Bikes. The histograms illustrate the detection error analysis performed with TIDE (Bolya et al., 2020).

One-Shot Target			
Method	person	bicycle	mAP
Baseline	69.0	74.1	71.6
$\gamma = 0$	Tran-Baseline	71.4	74.2
	OSHOT	68.9	74.6
	Tran-OSHOT	71.6	74.0
	Meta-OSHOT	69.5	73.5
	FULL-OSHOT	71.7	74.3
$\gamma = 5$	OSHOT	72.1	74.9
	Tran-OSHOT	73.0	74.7
	Meta-OSHOT	72.6	74.5
	FULL-OSHOT	73.3	75.1
Ten-Shot Target			
DivMatch (Kim et al., 2019b)	69.5	73.1	71.3
SW (Saito et al., 2019)	69.4	73.0	71.2
SW-ICR-CCR (Xu et al., 2020)	72.5	77.6	75.1
VDD-DAOD (Wu et al., 2021)	68.8	75.3	72.1
Whole Target			
DivMatch (Kim et al., 2019b)	73.6	77.1	75.4
SW (Saito et al., 2019)	68.6	70.3	69.5
SW-ICR-CCR (Xu et al., 2020)	72.0	72.8	72.4
ICCR-VDD (Wu et al., 2021)	71.1	71.9	71.5
Baseline			
Cl	25	25	25
Loc	20	20	20
Both	15	15	15
Dupe	10	10	10
Bkg	5	5	5
Miss	0	0	0
OSHOT $_{\gamma=0}$			
Cl	25	25	25
Loc	20	20	20
Both	15	15	15
Dupe	10	10	10
Bkg	5	5	5
Miss	0	0	0
OSHOT $_{\gamma=5}$			
Cl	25	25	25
Loc	20	20	20
Both	15	15	15
Dupe	10	10	10
Bkg	5	5	5
Miss	0	0	0
Tran-OSHOT $_{\gamma=5}$			
Cl	25	25	25
Loc	20	20	20
Both	15	15	15
Dupe	10	10	10
Bkg	5	5	5
Miss	0	0	0
Meta-OSHOT $_{\gamma=5}$			
Cl	25	25	25
Loc	20	20	20
Both	15	15	15
Dupe	10	10	10
Bkg	5	5	5
Miss	0	0	0
FULL-OSHOT $_{\gamma=5}$			
Cl	25	25	25
Loc	20	20	20
Both	15	15	15
Dupe	10	10	10
Bkg	5	5	5
Miss	0	0	0

of false negatives. Moreover, both *Tran-OSHOT* and FULL-OSHOT obtain a higher mAP than OSHOT thanks to lower *Miss* errors. The performance of FULL-OSHOT confirms that the meta-learning strategy with semantic-preserving data augmentations successfully prepares the model to solve the adaptation task at inference time.

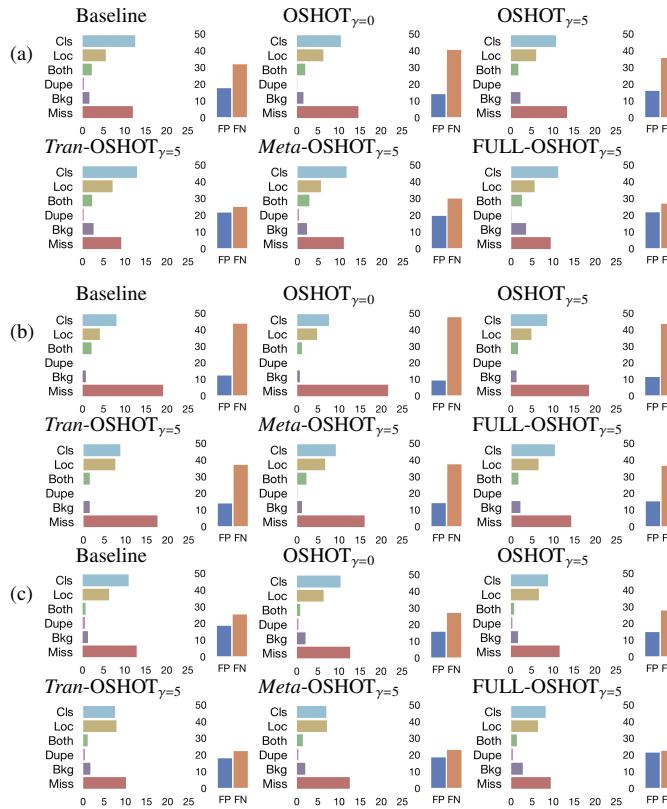
**Large distribution shifts.** Artistic images are difficult benchmarks for cross-domain methods. Unpredictable perturbations in shape and color are challenging to detectors trained only on real world photos. We investigate this setting by training on VOC and testing on Clipart, Comic and Watercolor datasets.

Table 2 shows that in all the three settings, by exploiting one sample at a time with few adaptive iterations ( $\gamma = 5$ ), OSHOT and its variants outperform the adaptive detectors despite they can leverage on ten target samples. More precisely, none of the adaptive detectors are able to work in data scarcity conditions and obtain results comparable to those of the *Tran-Baseline* and of the pretraining phase of our approach ( $\gamma = 0$ ). We also highlight that when  $\gamma = 5$ , *Meta-OSHOT* obtains results higher than *Tran-OSHOT* and only slightly lower on average than FULL-OSHOT, thus the meta-learning strategy alone (without additional data augmentation) prepares the detector to the inference time adaptation.

From the detection error analysis we see that the data augmentation of *Tran-OSHOT* pushes for a lower number of errors

Table 2: Results for VOC  $\rightarrow$  AMD and corresponding histograms with the error analysis performed with TIDE (Bolya et al., 2020).

(a) VOC $\rightarrow$ Clipart		(b) VOC $\rightarrow$ Comic		(c) VOC $\rightarrow$ Watercolor	
<b>One-Shot Target</b>		<b>One-Shot Target</b>		<b>One-Shot Target</b>	
Method	mAP	Method	mAP	Method	mAP
Baseline	26.4		18.1		42.8
Tran-Baseline	27.6		22.4		46.3
OSHOT	28.8		19.9		45.7
Tran-OSHOT	28.6		20.1		45.4
Meta-OSHOT	29.4		20.2		45.8
FULL-OSHOT	28.6		21.1		46.4
OSHOT	30.8		22.3		48.1
Tran-OSHOT	30.5		24.9		47.7
Meta-OSHOT	31.4		24.8		49.0
FULL-OSHOT	31.7		25.2		48.9
<b>Ten-Shot Target</b>		<b>Ten-Shot Target</b>		<b>Ten-Shot Target</b>	
DivMatch (Kim et al., 2019b)	26.3		20.8		45.4
SW (Saito et al., 2019)	26.4		21.0		42.0
SW-ICR-CCR (Xu et al., 2020)	27.2		21.1		45.3
ICCR-VDD (Wu et al., 2021)	27.6		24.8		43.1



of type *Miss*, while the meta learning strategy of *Meta-OSHOT* gets a lower number of *Classification* errors. *FULL-OSHOT* takes advantage of both, obtaining the best performance.

**Adverse weather.** Some environmental conditions, such as fog, may be disregarded in source data acquisition, yet adaptation to these circumstances is crucial in real world. We consider the Cityscapes  $\rightarrow$  FoggyCityscapes setting by training our base detector on the first domain. We perform model selection on the Cityscapes validation split before deployment.

The results in Table 3 show that domain adaptive detectors struggle in this scenario. Only SW-ICR-CCR and VDD-DAOD are able to exploit the small adaptation set and obtain a meaningful improvement over the Baseline. For what concerns OSHOT and its variants, the pretraining alone ( $\gamma = 0$ ) helps in

Table 3: Results for Cityscapes  $\rightarrow$  FoggyCityscapes. The histograms illustrate the detection error analysis performed with TIDE (Bolya et al., 2020).

<b>One-Shot Target</b>									
Method	person	rider	car	truck	bus	train	cycle	bicycle	mAP
Baseline	30.4	36.3	41.4	18.5	32.8	9.1	20.3	25.9	26.8
Tran-Baseline	32.1	35.2	42.9	17.8	31.0	4.3	22.6	30.0	27.0
OSHOT	32.2	38.6	39.0	20.5	30.6	12.9	22.4	31.2	28.4
Tran-OSHOT	30.5	37.4	42.7	16.9	29.5	14.5	21.9	30.4	28.0
$\gamma = 0$	30.6	35.1	35.9	16.6	28.4	7.6	18.2	28.4	25.1
FULL-OSHOT	31.7	40.8	43.7	18.3	28.8	11.0	22.8	33.3	28.8
OSHOT	32.7	39.3	41.1	21.1	33.1	12.6	22.7	31.9	29.3
Tran-OSHOT	30.9	38.5	43.0	17.5	32.1	13.9	21.6	30.5	28.5
$\gamma = 5$	32.1	38.2	39.9	17.4	30.9	7.5	21.0	29.2	27.0
FULL-OSHOT	32.0	39.7	43.8	18.8	31.8	10.6	22.1	33.2	29.0
<b>Ten-Shot Target</b>									
DivMatch (Kim et al., 2019b)	27.6	38.1	42.9	17.1	27.6	14.3	14.6	32.8	26.9
SW (Saito et al., 2019)	25.5	30.8	40.4	21.1	26.1	34.5	6.1	13.4	24.7
SW-ICR-CCR (Xu et al., 2020)	29.6	40.8	39.6	20.5	32.8	11.1	24.0	34.0	29.1
ICCR-VDD (Wu et al., 2021)	32.3	32.1	41.7	25.0	29.0	40.0	12.6	19.7	29.0
<b>Baseline</b>									
OSHOT $\gamma=0$	60	50	40	30	20	10	0	0	0
OSHOT $\gamma=5$	60	50	40	30	20	10	0	0	0
<b>Tran-OSHOT</b>									
OSHOT $\gamma=5$	60	50	40	30	20	10	0	0	0
Meta-OSHOT $\gamma=5$	60	50	40	30	20	10	0	0	0
FULL-OSHOT $\gamma=5$	60	50	40	30	20	10	0	0	0

Table 4: Comparison between baseline, one-shot style transfer and our approach in the one-shot unsupervised cross-domain detection setting. Speed computed on an RTX2080Ti with full precision settings.

	Baseline	BiOST (Cohen and Wolf, 2019)	OSHOT $\gamma = 5$	FULL-OSHOT $\gamma = 5$
mAP on Clipart100	27.9	29.8	28.2	30.4
mAP on Social Bikes	71.6	71.4	73.5	74.2
Adaptation time (s per sample)	-	$2.4 \times 10^4$	1.3	1.3

gaining a better generalization ability: all variants but *Meta-OSHOT* show higher performance than the Baseline. The advantage is also visible from the *Miss* error type which decreases when passing from the Baseline to OSHOT  $\gamma = 0$ , reaching its lower value for FULL-OSHOT with  $\gamma = 5$ .

**Comparison with One-Shot Style Transfer.** Although not designed for cross-domain detection, it is possible to apply one-shot style transfer methods as an alternative solution for our setting. We use BiOST (Cohen and Wolf, 2019), to modify the style of the target sample towards that of the source domain before performing inference. Due to the time-heavy requirements to perform BiOST on each test sample<sup>2</sup>, we test it on Social Bikes and on a random subset of 100 Clipart images that we name Clipart100. We compare performance and time requirements of our approach and BiOST on these two targets.

Table 4 shows the obtained mAP results. On Clipart100, the Baseline obtains 27.9 mAP. We can see how BiOST is effective as adaptation strategy from one-sample, gaining 1.9 points over the baseline. On Social Bikes, instead, BiOST incurs in a slight negative transfer, indicating its inability to effectively modify the source’s style on the images we collected. OSHOT improves over the baseline on Clipart100 but its mAP remains lower than that of BiOST, while it outperforms both the base-

<sup>2</sup>To get the style update, BiOST trains a double-variational autoencoder using the entire source besides the single target sample. As advised by the authors through personal communications we trained the model for 5 epochs.

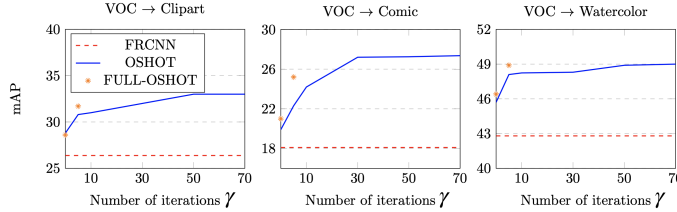


Fig. 3: Performance of OSHOT at different number of adaptive iterations.

line and BiOST on the more challenging Social Bikes. Finally, FULL-OShot shows the best results on both the datasets. The last row of the table presents the time complexity of all the considered methods, which is identical for OSHOT and FULL-OShot since the number of adaptive iterations is the same. BiOST instead, needs more than six hours to modify the style of a single source instance. Moreover we highlight that BiOST works under the strict assumption of accessing at the same time the entire source training set and the target sample. Considering these weaknesses and the obtained results, we argue that existing one-shot translation methods are not suitable for one shot unsupervised cross-domain adaptation.

**Increasing the number of Adaptive Iterations.** The bi-level optimization at the basis of meta-learning requires non-trivial computational and memory burdens that limit the feasible number of iterations  $\gamma$ . For FULL-OShot we use the same conditions for the meta pre-training and test time adaptation phases, thus we need to set a small number of training steps with  $\gamma = \eta$ . Differently for applications in which the number of iterations can be increased without time constraints, OSHOT appears better suited. We studied the performance of OSHOT in this case on the AMD dataset and collected the results in Figure 3. We observe a positive correlation between the number of finetuning iterations and the mAP of the model in the earliest steps, while the performance generally reaches a plateau after about 30 iterations: increasing  $\gamma$  beyond this value does not affect significantly the final results. In the plots we represent with orange stars the performance of FULL-OShot at 0 and 5 adaptation iterations. We can see that FULL-OShot has quite better performance w.r.t. OSHOT when they are both tested with 5 adaptation iterations, while OSHOT might outperform FULL-OShot with a significant longer learning period.

## 5. Conclusion

This paper focused on one-shot unsupervised cross-domain detection, where adaptation should be performed on one single image at inference time, without access to the source data. This scenario mimicks the conditions encountered for real world applications like social media monitoring. We showed how our FULL-OShot outperforms several cross-domain detection methods and improves over its basic OSHOT version (D’Innocente et al., 2020) thanks to a novel meta-learning formulation applied on the auxiliary self-supervised task: this procedure simulates single-sample cross-domain learning episodes and improves the generalization abilities of the detector.

## References

Alliegro, A., Boscaini, D., Tommasi, T., 2021. Joint supervised and self-supervised learning for 3d real world challenges, in: ICPR.

Asano, Y.M., Rupprecht, C., Vedaldi, A., 2020. A critical analysis of self-supervision, or what we can learn from a single image, in: ICLR.

Balaji, Y., Sankaranarayanan, S., Chellappa, R., 2018. Metareg: Towards domain generalization using meta-regularization, in: NeurIPS.

Bolya, D., Foley, S., Hays, J., Hoffman, J., 2020. Tide: A general toolbox for identifying object detection errors, in: ECCV.

Bucci, S., D’Innocente, A., Liao, Y., Carlucci, F.M., Caputo, B., Tommasi, T., 2021. Self-supervised learning across domains. IEEE TPAMI .

Chen, Y., Li, W., Sakaridis, C., Dai, D., Van Gool, L., 2018. Domain adaptive faster r-cnn for object detection in the wild, in: CVPR.

Cohen, T., Wolf, L., 2019. Bidirectional one-shot unsupervised domain mapping, in: ICCV.

Cordts, M., Omran, M., Ramos, S., Rehfeld, T., Enzweiler, M., Benenson, R., Franke, U., Roth, S., Schiele, B., 2016. The cityscapes dataset for semantic urban scene understanding, in: CVPR.

D’Innocente, A., Borlino, F.C., Bucci, S., Caputo, B., Tommasi, T., 2020. One-shot unsupervised cross-domain detection, in: ECCV.

Everingham, M., Van Gool, L., Williams, C.K., Winn, J., Zisserman, A., 2010. The pascal visual object classes (voc) challenge. IJCV 88, 303–338.

Finn, C., Abbeel, P., Levine, S., 2017. Model-agnostic meta-learning for fast adaptation of deep networks, in: ICML.

Hoffman, J., Darrell, T., Saenko, K., 2014. Continuous manifold based adaptation for evolving visual domains, in: CVPR.

Inoue, N., Furuta, R., Yamasaki, T., Aizawa, K., 2018. Cross-domain weakly-supervised object detection through progressive domain adaptation, in: CVPR.

Khodabandeh, M., Vahdat, A., Ranjbar, M., Macready, W.G., 2019. A robust learning approach to domain adaptive object detection, in: ICCV.

Kim, S., Choi, J., Kim, T., Kim, C., 2019a. Self-training and adversarial background regularization for unsupervised domain adaptive one-stage object detection, in: ICCV.

Kim, T., Jeong, M., Kim, S., Choi, S., Kim, C., 2019b. Diversify and match: A domain adaptive representation learning paradigm for object detection, in: CVPR.

Li, Y., Yang, Y., Zhou, W., Hospedales, T., 2019. Feature-critic networks for heterogeneous domain generalization, in: ICML.

Lin, T.Y., Goyal, P., Girshick, R., He, K., Dollar, P., 2017. Focal loss for dense object detection, in: ICCV.

Mancini, M., Karaoguz, H., Ricci, E., Jensfelt, P., Caputo, B., 2018. Kitting in the wild through online domain adaptation, in: IROS.

Motiani, S., Jones, Q., Iranmanesh, S., Doretto, G., 2017. Few-shot adversarial domain adaptation, in: NIPS.

Ren, S., He, K., Girshick, R., Sun, J., 2015. Faster r-cnn: Towards real-time object detection with region proposal networks, in: NIPS.

Rusu, A.A., Rao, D., Sygnowski, J., Vinyals, O., Pascanu, R., Osindero, S., Hadsell, R., 2019. Meta-learning with latent embedding optimization, in: ICLR.

Saito, K., Ushiku, Y., Harada, T., Saenko, K., 2019. Strong-weak distribution alignment for adaptive object detection, in: CVPR.

Sakaridis, C., Dai, D., Van Gool, L., 2018. Semantic foggy scene understanding with synthetic data. IJCV 126, 973–992.

Snell, J., Swersky, K., Zemel, R., 2017. Prototypical networks for few-shot learning, in: NeurIPS.

Tobin, J., Fong, R.H., Ray, A., Schneider, J., Zaremba, W., Abbeel, P., 2017. Domain randomization for transferring deep neural networks from simulation to the real world, in: IROS.

Tseng, H.Y., Lee, H.Y., Huang, J.B., Yang, M.H., 2020. Cross-domain few-shot classification via learned feature-wise transformation, in: ICLR.

Vinyals, O., Blundell, C., Lillicrap, T., kavukcuoglu, k., Wierstra, D., 2016. Matching networks for one shot learning, in: NeurIPS.

Wu, A., Liu, R., Han, Y., Zhu, L., Yang, Y., 2021. Vector-decomposed disentanglement for domain-invariant object detection, in: ICCV.

Xu, C.D., Zhao, X.R., Jin, X., Wei, X.S., 2020. Exploring categorical regularization for domain adaptive object detection, in: CVPR.

Xu, J., Xiao, L., López, A.M., 2019. Self-supervised domain adaptation for computer vision tasks. IEEE Access 7:1-1.